Optical properties of nanostructures

V.K.Miloslavsky, L.A.Ageev, E.D.Makovetsky, S.A.Maskevich[*]

V.Karazin Kharkiv National University, 4 Svobody sq.,
Kharkiv, 61077, Ukraine
*Ya.Kupala Grodno State University, 22 Ozheshko st.,
Grodno, 230023, Belarus

The paper is a brief review of optical properties of nanostructures containing metal nanoparticles. There is a deduction of some simple formulae describing optical spectra of composites containing small particles of various form. Comparison of theoretical and experimental data has been carried out. Conclusions following Mie theory of diffraction on spheres of various diameters and dielectric permittivities are discussed. Various examples of applications of nanoparticles and their influence on surrounding media are given.

Представлен краткий обзор оптических свойств наноструктур, содержащих металлические наночастицы. Приведены выводы некоторых простых формул, используемых для описания оптических спектров композитов, содержащих малые частицы различной формы. Проведено сравнение теории с данными эксперимента. Обсуждаются следствия, вытекающие из теории Ми, посвященной дифракции на сферах различного диаметра и с различной диэлектрической проницаемостью. Приведены разнообразные примеры практического применения наночастиц и их воздействия на окружающую среду.

Introduction

The search for new materials for semiconductor electronics and optoelectronics has led during last decades to study of solid composites containing small particles of different materials, referred to as nanoparticles. But what does the term "nanoparticle" mean? At first glance, the answer seems to be easy: "nanoparticle" implies particle diameter d of dozens or units of nanometers. In that case, d is substantially smaller than visible light wavelengths λ (about 500 nm). The optical and other properties of composites containing such nanoparticles should differ from those of corresponding dielectric matrices and bulk materials of which the nanoparticles consist. As a first approximation, optical properties of the composite may be described using an effective dielectric permittivity assuming that, first, at $d << \lambda$ the composite behaves as an optically homogeneous medium [1–3], and second, the Rayleigh scattering (typical of homogeneous media) may be neglected when measuring transmission. Such a conclusion may be drawn for dielectrics containing metal or semiconductor particles with $d \leq 20$ nm [1, 2].

On the other hand, composites may have a semiconductor matrix with a relatively narrow band gap E_g. The transparency region of such semiconductors lies within infrared range ($l \approx 1 \div 100 \mu$m). If the nanoparticles are made of semiconductors or metals, then resonance absorption bands of composites are situated at $\hbar\omega < E_g$, and the criterion of particle smallness ($d << \lambda$) is met for particles with $d \approx 100$ nm. As to semiconductor conductive particles with $E_g \leq 1$ eV a quantum size effect is typical, so their dielectric permittivity may differ substantially from that of bulk semiconductor (quantum dots). Numerous works have been aimed at study of various properties of such composites

in connection with their use in novel semiconductor devices, in particular, lasers [4, 5].

In this review, the attention will be focused on "classical" nanostructures: composites with dielectric matrices containing metal particles. Many properties of nanostructures are explainable basing on classical electrodynamics, taking into consideration size and form of nanoparticles. Experimental data on optical properties of such composites (absorption spectra, dichroism) have been compared with theoretical conclusions. Some aspects of composite use should be accentuated. Nanostructures play a significant part in photographic process [6] and in chemistry of colloidal solutions [7]. They are used for coloration of transparent matrices (glasses and crystals), for manufacturing dichroic polarizers and for other purposes. Nanostructures are also formed in thin metal films and define the optical and electronic properties thereof differing from those of bulk metals [8, 9]. The electromagnetic fields being generated by nanoparticles influence substantially the surrounding, cause excitation of surface plasmons in metals [10], affect the external photoeffect [9] and nonlinear optical properties of media [10], result in a substantial amplification of Raman light scattering by molecules contacting with nanoparticles [11]. Lately, nanoparticles are becoming a part of everyday life. They are used in manufacturing clothes with new properties, various pastes, etc. [12]. A special new international journal named "Photonics and Nanostructures – Fundamentals and Applications" is being published since December 2003.

Optical Properties of Small Metal Spheres

As small metal particles, we will consider the particles of radius a considerably smaller than the light wavelength λ. The criterion of smallness is $k \cdot a << 1$ where $k = \dfrac{2\pi}{\lambda} \cdot n_0$ is the wave vector of light in surrounding medium. The criterion being fulfilled, scattering is substantially smaller than absorption and may be neglected. The particles in matrix may have various shapes. In many cases, they are spherical favored by minimum of surface energy. Anisometric particles of size answering the smallness criterion, and particles of more complex form are also considered.

Let a small spherical particle be located in a transparent isotropic dielectric with permittivity ε_0. Let us also assume that the metal particle is isotropic and has a permittivity $\varepsilon = \varepsilon_1 - i\varepsilon_2$. Further, we assume the particles in composite medium to be identical and to be spaced by distances exceeding considerably λ. At such conditions, interaction of secondary fields (generated by adjacent particles) may be neglected. It is enough to consider the light attenuation by a separate particle and then to sum up the intensities of light passed through an ensemble of particles at a specified concentration. The smallness criterion being met, the spatial phase part of the wave penetrating the particle can be neglected, thus, the electrostatic approximation is realized. In other words, the electric field strength inside the particle is independent of coordinates and oscillates with the frequency of incident monochromatic wave.

Since the sphere is situated in the medium with permittivity ε_0, the field affecting the electrons in metal differs from the field E outside the sphere and is [13]

$$E' = \frac{3\varepsilon_0}{1 + 2\varepsilon_0} \cdot E - \frac{4\pi}{1 + 2\varepsilon_0} \cdot P, \tag{1}$$

where $P = N \cdot p$ is the dipole moment of unit volume in the sphere; N, the concentration of electrons; p, the dipole moment induced at a single electron displacement. Let us assume that only free electrons are shifted due to action of the field E', while displacement of electrons connected with ions may be neglected. The equation of stimulated electron oscillations under action of field with frequency ω has the form

$$\ddot{p} + \nu \cdot \dot{p} = \frac{e^2}{m}\left(\frac{3\varepsilon_0}{1 + 2\varepsilon_0} \cdot E - \frac{4\pi}{1 + 2\varepsilon_0} \cdot P \right), \tag{2}$$

where ν is frequency of electron scattering. We will look for solution in the form $p = p_0 \exp(i\omega t)$

using the relationship $P = N \cdot p$. In that case, the equation (2) is reduced to an algebraic one:

$$\left(-\omega^2 + i\nu\omega + \frac{\omega^2}{1+2\varepsilon_0} \right) \cdot P = \frac{3\varepsilon_0 \omega_{\mathrm{p}}^2}{4\pi(1+2\varepsilon_0)} \cdot E , \tag{3}$$

where $\omega_{\mathrm{p}} = \sqrt{4\pi N e^2/m}$ is the plasma frequency.

Let a composite medium to contain N_0 of identical spheres with volume V. The specific volume occupied by spheres in dielectric (the filling factor) is $q = N_0 \cdot V$. The effective permittivity of the medium may be written as

$$\varepsilon_{\mathrm{ef}} = \varepsilon_0 (1-q) + q \left(1 + \frac{4\pi P}{E} \right). \tag{4}$$

Here the Newton formula for $\varepsilon_{\mathrm{ef}}$ of mixture [2] is used:

$$\varepsilon_{\mathrm{ef}} = \varepsilon_{\mathrm{mix}} = \varepsilon_1 (1-q) + \varepsilon_2 q .$$

Substituting (3) into (4) results in

$$\varepsilon_{\mathrm{ef}} = \varepsilon_0 (1-q) + q \cdot \left\{ 1 + \frac{3\varepsilon_0 \omega_{\mathrm{p}}^2}{(1+2\varepsilon_0) \cdot (-\omega^2 + i\nu\omega) + \omega_{\mathrm{p}}^2} \right\}. \tag{5}$$

The complex dielectric permittivity of bulk metal in a wide frequency range is defined by well-known Drude-Lorenz formula [14]:

$$\varepsilon' = 1 + \frac{\omega_p^2}{-\omega^2 + i\nu\omega} . \tag{6}$$

Using (6), let the factor $(-\omega^2 + i\nu\omega)$ in denominator of (5) be replaced by $\omega_p^2/(\varepsilon' - 1)$. After some transformations, we obtain the final formula for $\varepsilon_{\mathrm{ef}}$ of a mixture containing metal spheres:

$$\varepsilon_{\mathrm{ef}} = \varepsilon_0 + q \cdot (1+2\varepsilon_0) \frac{\varepsilon' - \varepsilon_0}{\varepsilon' + 2\varepsilon_0} . \tag{7}$$

Due to complexity of ε', the permittivity of mixture is also complex: $\varepsilon_{\mathrm{ef}} = \varepsilon_{\mathrm{1ef}} - i\varepsilon_{\mathrm{2ef}}$. Separating real and imaginary parts of ε', we get

$$\varepsilon_{\mathrm{1ef}} = \varepsilon_0 + q \frac{(1+3\varepsilon_0)(\varepsilon_1^2 + \varepsilon_2^2 + 2\varepsilon_1\varepsilon_0)}{(\varepsilon_1 + 2\varepsilon_0)^2 + \varepsilon_2^2} , \quad \varepsilon_{\mathrm{2ef}} = q \frac{3\varepsilon_0(1+2\varepsilon_0)\varepsilon_2}{(\varepsilon_1 + 2\varepsilon_0)^2 + \varepsilon_2^2} \tag{8a,b}$$

where, basing on (6),

$$\varepsilon_1 = 1 - \frac{\omega_{\mathrm{p}}^2}{\omega^2 + \nu^2} , \quad \varepsilon_2 = 1 - \frac{\omega_{\mathrm{p}}^2 \cdot \nu}{\omega(\omega^2 + \nu^2)} . \tag{9}$$

It should be noted that inequality $\omega \gg \nu$ is valid in visible and UV frequency range for most metals, as $\omega \approx 10^{15} \, \mathrm{s}^{-1}$ and $\nu \approx 10^{13} \div 10^{14} \, \mathrm{s}^{-1}$. Therefore, ν^2 in (9) may be neglected. Let us substitute ε_1 and ε_2 into $\varepsilon_{\mathrm{2ef}}$:

$$\varepsilon_{\mathrm{2ef}} = 3q\varepsilon_0(1+2\varepsilon_0) \frac{\omega_{\mathrm{p}}^2 \nu \omega^3}{[(1+2\varepsilon_0)\omega^2 - \omega_{\mathrm{p}}^2]^2 \omega^2 + \omega_{\mathrm{p}}^4 \nu^2} . \tag{10}$$

Basing on (10) one can conclude that maximum of $\varepsilon_{\mathrm{2ef}}$ is at the frequency

$$\omega_{\mathrm{F}} = \frac{\omega_{\mathrm{p}}}{\sqrt{1+2\varepsilon_0}} . \tag{11}$$

This is the so-called Frölich frequency. At $\omega = \omega_F$,

$$\varepsilon_{2ef}^{max} = \frac{3q\varepsilon_0}{\sqrt{1+2\varepsilon_0}} \cdot \frac{\omega_p}{\nu} . \tag{12}$$

Dependence $\varepsilon_{2ef}(\omega)$ has a contour close to the Lorentz one. The contour half-width $\Delta\omega$ (the width at half height) is defined by frequencies

$$\omega_{1,2} = \omega_F \pm \frac{\nu}{2\sqrt{1+2\varepsilon_0}} , \quad \Delta\omega = \frac{\nu}{\sqrt{1+2\varepsilon_0}} . \tag{13}$$

The presented calculation is based on assumption that only free electrons are shifted under action of light wave field. Such an assumption is suitable for alkali elements having the interband absorption edge in far UV region, and it may be used in study of colloidal solutions of alkali elements in alkali halide crystals [15]. Many metals, however, have the low-frequency edge of interband transition in near UV and visible regions. Those are noble metals (Cu, Ag, Au) and a number of metals of the Fe and Pt group. The edge of interband transitions in Cu and Au is situated in visible spectral region. This fact defines the reflection spectra and colors thereof.

Optical interband transitions in metals create continuous bands, absorption and reflection of metals is calculated using the complex permittivity ε'. Basing on classical dispersion theory, the frequency dependence $\varepsilon'(\omega)$ in the bands can be described using a set of susceptibilities of harmonic oscillators [1]:

$$\varepsilon' = 1 + \sum_{i=1}^{n} \frac{\omega_{p_i}^2}{\omega_{0_i}^2 - \omega^2 + i\nu_{0_i}\omega} , \tag{14}$$

where ω_{0_i} is the i-th transition natural frequency, $\omega_{p_i}^2 = 4\pi N_i e^2/m$, N_i is the number of electrons participating in the i-th transition. For metals, the sum in (14) includes the summand related with free electrons ($\omega_{0_i} = 0$). If the metal is nanometer-scaled sphere immersed into transparent dielectric, then, taking into consideration the acting field E' (see (1)) and polarization $P = \sum_i N_i p_i$, the stimulated oscillation equation of the family of oscillators can be presented as algebraic equations [16]:

$$(-\omega^2 + i\nu_{0_i}\omega + \omega_{0_i}^2 + \omega_{s_i}^2)p_i + \sum_{j\neq i}^{n-1} \omega_{s_j}^2 p_j = \frac{3\varepsilon_0 e^2}{m(1+2\varepsilon_0)} \cdot E , \tag{15}$$

where $\omega_{s_i}^2 = \dfrac{\omega_{p_i}^2}{1+2\varepsilon_0}$. The system of n equations may be solved using common solution rules for equations with a right-hand member. As a result, we get p_i, $P = \sum_i N_i p_i$, and effective permittivity of mixture using (4) and (14):

$$\varepsilon_{ef}(\omega) = \varepsilon_0(1-q) + q\left\{1 + 3\varepsilon_0 \frac{\sum_i\left(\omega_{s_i}^2 \prod_{j\neq i} r_j'\right)}{\prod_i r_i' + \sum_i\left(\omega_{s_i}^2 \prod_{j\neq i} r_j'\right)}\right\} , \tag{16}$$

where the complex value $r_i' = \omega_{0_i}^2 - \omega^2 + i\nu_{0_i}\omega$, $\prod_i$ is notation for a product. The formula (16) allows natural frequencies to be redefined due to dimensional quantization in a sphere and change of ν_{0_i} due to electron scattering on the sphere surface. If the oscillator characteristics in spheres and in the bulk material are the same, then, as follows from (14) and (16), $\varepsilon_{ef}(\omega)$ is reduced to (7):

$$\varepsilon_{ef} = \varepsilon_0 + q(1+2\varepsilon_0)\frac{\varepsilon'-\varepsilon_0}{\varepsilon'+2\varepsilon_0} , \tag{17}$$

but ε' is now defined by (14). Having assumed the right-hand member of (15) to be zero, we proceed to n self-oscillation equations of a system including n oscillators. The oscillation natural frequencies in a small sphere are obtained by solving the secular equation

$$\mathrm{Re}\left(\det\left|r_i'\delta_{ij} + \omega_{s_j}^2\right|\right) = 0 , \tag{18}$$

where δ_{ij} is the Kronecker symbol. Due to presence of non-diagonal elements in (18) the i-th oscillator natural frequency differs from $\sqrt{\omega_{0_i}^2 + \omega_{s_i}^2}$, i.e. a combined (hybrid) resonance occurs in the metal sphere. There is a complicated dependence of resonance frequencies on characteristics of all the oscillators defining optical behavior of bulk metal. The equation (18) is reduced to

$$1 + \sum_i \frac{\omega_{p_i}^2\left(\omega_{0_i}^2 - \omega^2\right)}{\left(\omega_{0_i}^2 - \omega^2\right)^2 + \nu_{0_i}^2\omega^2} = -2\varepsilon_0 . \tag{19}$$

It follows from (14) that the right part of (19) is the real part of $\varepsilon' = \varepsilon_1 - i\varepsilon_2$, i.e. equation for ω_i has the form $\varepsilon_1(\omega) = -2\varepsilon_0$. As the sum in (19) includes the item associated with free electrons, let their oscillation natural frequency in sphere ω_1 be found. In this case, (19) takes the form

$$1 + \Delta\varepsilon_1(\omega_1) - \frac{\omega_{p_1}^2}{\omega_1^2} = -2\varepsilon_0 , \tag{20}$$

where $\sqrt{\Delta\varepsilon_1(\omega_1)}$ is the part of sum in (19) at $i \neq 1$. As frequency ω_1 in $\Delta\varepsilon_1$ differs substantially from ω_{0_i}, the weak dependence of $\Delta\varepsilon_1$ on ω_1 may be neglected, and natural frequency $\omega_1 = \omega_F$ is

$$\omega_F = \frac{\omega_{p_1}}{\sqrt{1 + \Delta\varepsilon_1(\omega_1) + 2\varepsilon_0}} = \frac{\omega_{p_1}}{\sqrt{\varepsilon_M(\omega_1) + 2\varepsilon_0}} , \tag{21}$$

where ω_{p_1} is the plasma frequency of free electrons. It follows from (21) that the Frölich frequency in a real metal may differ substantially from formula (11) derived assuming absence of electron shift associated with optical interband transitions. Thus, $\varepsilon_M = 4.5$ for Ag [17], $\varepsilon_M = 6.5$ for Au [2]. The calculation shows that ω_F shifts noticeably as ε_M is taken into account. The plasma frequency of Ag is $\omega_p = 1.35 \cdot 10^{16}\,\mathrm{s}^{-1}$, and calculation of ω_F results in values $4.5 \cdot 10^{15}\,\mathrm{s}^{-1}$ from (21) and $5.7 \cdot 10^{15}\,\mathrm{s}^{-1}$ according to (11).

The formula (17) is derived for ε_{ef} of small spherical particles in a dielectric. As it follows from (17), the spectral position of resonance band maximum ω_F is independent of the filling factor

$$q = N_0 V . \tag{22}$$

At the same time, experiment [2] evidences a noticeable low-frequency shift of resonance bands as q increases. The shift may be caused by q increase due to the particle volume V. The particle radius a increasing, the smallness criterion $k \cdot a \ll 1$ becomes broken. The quasi-static approximation at $k \cdot a \approx 1$ is no longer suitable, and one should use Mie theory [1, 7, 18] to calculate the natural frequencies. Moreover, the Mie theory predicts increase of light scattering by particles as V increases, and attenuation of light beam passing through the solution of spheres is due not only to absorption but to scattering, too. If that is the case, the conception of the solution ε_{ef} loses sense.

On the other hand, increase of q at small radii of spheres may be due to increasing concentration of spheres N_0. In that case, the frequency shift may be caused by influence of secondary fields generated by particles adjacent to the specified one. While summing with external field, secondary fields modify the field acting on electrons in the specified particle. The criterion $k \cdot a \ll 1$ is kept, and colloidal solution may be considered as an optically homogeneous medium with an effective

permittivity ε_{ef} . A number of formulae is suggested for such a medium (see [2]), the Maxwell-Garnett one [19] being the most widely used:

$$\frac{\varepsilon_{ef} - \varepsilon_0}{\varepsilon_{ef} + 2\varepsilon_0} = q \frac{\varepsilon' - \varepsilon_0}{\varepsilon' + 2\varepsilon_0} . \tag{23}$$

The formula (23) is derived basing on the Lorenz-Lorentz formula [18] taking into account the field acting on dipoles (molecules) surrounded by sphere. It may be reduced to (17) at replacing ε_{ef} by 1 in the left part denominator of (23).

The formula (23) has an advantage as compared to (17). First, it predicts a low-frequency shift as q increases [2]. Second, it makes sense as an interpolation formula, and at $q = 1$, it gives $\varepsilon_{ef} = \varepsilon'$ i.e. the bulk metal permittivity. As calculation using (23) shows, the imaginary part of ε_{ef} is

$$\varepsilon_{2ef} = \frac{9\varepsilon_0^2 \varepsilon_2 \cdot q}{\left[\varepsilon_1 + 2\varepsilon_0 - (\varepsilon_1 - \varepsilon_0)q\right]^2 + \varepsilon_2^2(1 - q)^2} , \tag{24}$$

and at small q it is reduced to formula (8b) accurate to within the multiplier $3\varepsilon_0/(1 + 2\varepsilon_0)$. It follows from (24) that at $q \to 0$, frequency dependence of ε_{2ef} is defined by a contour close to the Lorentz one, and maximum of colloidal absorption band is located at Frölich frequency (21). The formula (24) describes results of experiments in porous media rather well if pores have a spherical form and small radii, and if the filling factor of pores in absorbing medium $q' = 1 - q$ has a small value. This may be exemplified by optical properties study of porous silicon [5].

In the case of $q \approx 0.5$, the concept of continuous matrix with minute spheres dissolved or pores formed, loses sense, and it is preferable to use the Bruggermann formula [20] to describe optical properties of such a medium:

$$q \frac{\varepsilon' - \varepsilon_{ef}}{\varepsilon' + 2\varepsilon_{ef}} + (1 - q)\frac{\varepsilon_0 - \varepsilon_{ef}}{\varepsilon_0 + 2\varepsilon_{ef}} = 0 , \tag{25}$$

where ε' and ε_0 are permittivities of metal and dielectric, respectively. Formula (25) is derived under the assumption of an effective medium consisting of almost contacting spheres, and average field in the medium $\bar{E} = qE_1' + (1 - q)E_2'$ includes fields acting on electrons in every sphere with ε' and ε_0. Just as Maxwell-Garnett formula, the (25) is an interpolation one, as $\varepsilon_{ef} = \varepsilon_0$ at $q = 0$ and $\varepsilon_{ef} = \varepsilon'$ at $q = 1$. It should be noted that at $q \to 0$ formula (25) is reduced to the Maxwell-Garnett one but it gives different results at intermediate q values. It is assumed [5] that (25) agrees better with experiment than (23) at $0.33 \leq q \leq 0.67$.

The applicability of formulae (17) and (23) is demonstrated by the following experiment [21]. Thin film of Ag (about 10 nm) was applied onto amorphous quartz plate by vacuum deposition. Then the sample was irradiated by continuous beam of a CO_2-laser ($\lambda = 10.6\mu m$, $P \approx 30W$). The irradiated sample part was heated up to approximately 1000°C in nearly 1 min. The irradiation resulted in yellow coloration of 3–4 mm diameter area. The coloration evidences penetration of minute Ag particles into the quartz surface layer. Sulphuric acid solution treatment did not result in coloration disappearance or decolorizing, thus confirming Ag penetration into quartz.

It was established by electron and AFM microscopy that bulges were formed on quartz surface having average height of about 5 nm and average spacing of about 0.5 μm. Spectrophotometric measurements have shown that Ag particles in quartz create a relatively thin absorption band with maximum at 420 nm ($\hbar\omega_m = 2.95\,eV$) and with contour close to the Lorentz one. It was established that ω_m is close to the Frölich frequency (21) at $\hbar\omega_p = 8.85\,eV$, $\varepsilon_M(\omega_m) = 4.5$ [17], $\varepsilon_0 = 2.15$ for quartz. Data processing for the absorption band of colloidal Ag in quartz using (23) (Fig.1, [22]) has shown that the band half-width γ is substantially larger than that calculated basing on data obtained at Ag optical constants measurements ($\nu = 4.3 \cdot 10^{13}\,s^{-1}$). The reason of increased electron scattering is the scattering on particle boundaries. The γ value in that case may be estimated as
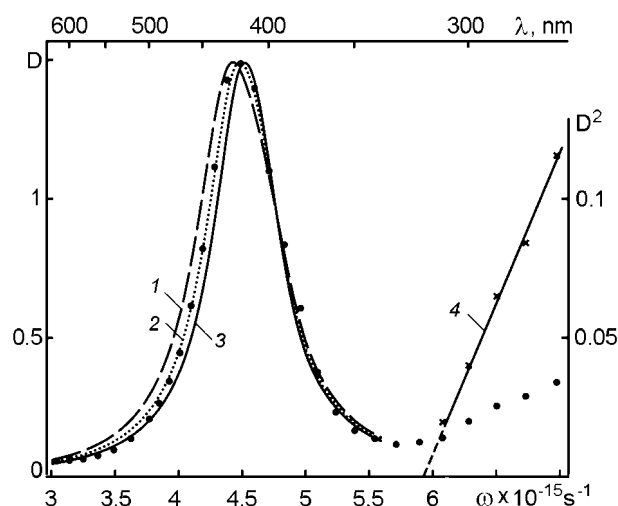
Fig.1. Absorption spectra $D(\omega)$ is displayed by experimental points; *1*, *2*, and *3* are the calculated contours $D(\omega)$ with $q = 0.15, 0.10, 0.05$, respectively; *4*, the experimental dependence $D^2(\omega)$.

$$\gamma = \nu + k \cdot \frac{V_F}{a} \qquad (26)$$

where constant factor k is close to 1, V_F is electron speed at Fermi surface ($V_F = 2.3 \cdot 10^8$ cm $\cdot$ s^{-1} for Ag), a is sphere radius. For the γ value found at $k = 1$, the value $a \approx 3$ nm was obtained that is in agreement with AFM and electron microscopy results. Calculation using (23) and experimental data agree in the best way at $q = 0.1$. Since the optical density at the absorption band maximum $D = K_{ef} \cdot d$, where d is thickness of the layer alloyed by silver and $K_{ef} = \dfrac{2\omega}{C} \cdot \dfrac{\varepsilon_{2ef}}{\sqrt{\varepsilon_0}}$ is absorption coefficient, the q value resulted in $d \approx 50$ nm.

Being exposed to air or another oxidative media, many metals get covered by thin dielectric films. The films often have nanometer scale thickness and impede further oxidation. In this connection, it is of interest to study optical properties of aerosols and colloidal solutions consisting of small spherical metal particles surrounded with a dielectric coating. Calculation of polarizability of such particles [23, 24] provides the effective permittivity of solution:

$$\varepsilon_{ef} = \varepsilon_0 + q(1 + 2\varepsilon_0) \frac{(\varepsilon_1 + 2\varepsilon_2)(\varepsilon_2 - \varepsilon_0) + p^3(\varepsilon_1 - \varepsilon_0)(2\varepsilon_2 + \varepsilon_0)}{(\varepsilon_1 + 2\varepsilon_2)(\varepsilon_2 + 2\varepsilon_0) + 2p^3(\varepsilon_1 - \varepsilon_2)(\varepsilon_2 - \varepsilon_0)}, \qquad (27)$$

where ε_1, ε_2, ε_3 are permittivities of metal core of sphere ($\varepsilon_1 \equiv \varepsilon'$), of dielectric coating and surrounding medium, respectively, $q = N_0 V$, V is the sphere total volume, p is ratio of core radius to sphere radius. As follows from (27), at $p = 0$ (i.e. at absence of core), there is ε_{ef} of dielectric spheres in surrounding matrix while at $p = 1$ (i.e. at absence of coating), Eq. (27) is reduced to (7).

As an example, we cite an experiment on AgI coating formation on Ag spheres [25]. Thin Ag film was deposited on a smooth glass surface heated up to 300°C. Electron microphotographs revealed formation of spherical granules, and absorption band with maximum at $\omega_{0_m} = 4.2 \cdot 10^{15}$ s^{-1} appeared. Calculation of ω_{0_m} at $\varepsilon_0 = 1$ resulted in $\omega_{0_m} = \dfrac{\omega_p}{\sqrt{\varepsilon_M + 2}} = 5.25 \cdot 10^{15}$ s^{-1}. The difference between calculated and experimental ω_{0_m} values evidences a considerable shift of absorption band due to large q. Then the sample was treated by I_2 vapors. Iodination changed the film coloration from yellow to blue one. Transmission measurements showed that during initial stages of iodination the band shifts to lower frequencies, then shifting slows down, and the band is weakened when its maximum is at $\omega_m = 3.25 \cdot 10^{15}$ s^{-1}. As it follows from (27) taking into account (9), the resonance frequency at AgI coating formation is

$$\omega_m^2 = \omega_{0_m}^2 \frac{(\varepsilon_M + 2)(\varepsilon_2 + b)}{\varepsilon_2(\varepsilon_M + 2) + b(\varepsilon_M + 2\varepsilon_2)}, \qquad (28)$$

where $b = (1 - p^3)(\varepsilon_2 + 2)/3p^3$, ε_M is the real part of ε' associated with interband transitions. At small p (core reduced at the expense of coating), $\omega_m \to \omega_m = \dfrac{\omega_p}{\sqrt{\varepsilon_M + 2\varepsilon_2}}$. This formula corresponds

to a small sphere in AgI matrix ($\varepsilon_2 = 4.9$). Calculation results in the value $\omega_m = 3.54 \cdot 10^{15} \, s^{-1}$ close to experimental one $\omega_m = 3.25 \cdot 10^{15} \, s^{-1}$.

Optical Properties of Anisometric Particles

Nanostructures may also include anisometric metal particles, elongated spheroids or discoid ones. Those can be exemplified by dichroic polarizers containing minute absorbing anisometric particles [7, 26], glasses containing metal particles and subjected to uniaxial compression [2], anisometric nanoparticles in photosensitive layers irradiated by polarized light [6], etc. In this connection, there is an interest in optical properties and absorption spectra of composite media containing anisometric particles.

Let an isotropic transparent matrix to contain anisometric particles being metal ellipsoids that are substantially smaller than λ and have an uniform orientation. Let such a particle to be affected by linearly polarized light with vector $\mathbf{E}$ oriented along one of principal axes α of the ellipsoid. Then electrons in metal are shifted by x_{i_α}, and equation of stimulated electron oscillations takes the form [27]

$$\ddot{x}_{i_\alpha} + \nu_{0_i} \dot{x}_{i_\alpha} + x_{i_\alpha} \omega_{0_i}^2 = \frac{e}{m} E_\alpha', \tag{29}$$

where ω_{0_i}, ν_{0_i} are natural frequencies and attenuation frequencies of electrons involved in i-th interband transition. At $\omega_{0_i} = 0$, the equation (29) concerns free electrons, E_α' is an effective field acting on electrons:

$$E_\alpha' = \frac{\varepsilon_0 E_\alpha}{\varepsilon_0 - L_\alpha (\varepsilon_0 - 1)} - \frac{4\pi L_\alpha P_\alpha}{\varepsilon_0 - L_\alpha (\varepsilon_0 - 1)}, \tag{30}$$

where $P_a = \sum_i e N_i x_{i_a}$ is polarization of electrons in ellipsoid, L_α are depolarizing factors. The latter are associated with ellipsoid principal axis lengths a, b, c, and $\sum_{\alpha=1}^{3} L_\alpha = 1$. The L_1 value is different for elongated and flattened ellipsoids, $a \neq b = c$. For elongated ellipsoids ($a > b$) [7]

$$L_1 = \frac{1 - e^2}{e^2} \left(-1 + \frac{1}{2e} \ln \frac{1+e}{1-e} \right), \quad e^2 = 1 - \frac{b^2}{a^2}, \tag{31}$$

for flattened ellipsoids ($a < b$)

$$L_1 = \frac{1 + g^2}{g^2} \left(1 - \frac{1}{g} \arctan(g) \right), \quad g^2 = \frac{b^2}{a^2} - 1. \tag{32}$$

At a close to b, $L_1 = \frac{1}{3} + \frac{4}{15} \cdot \frac{b-a}{a}$. At $b = a$ (sphere), $L_1 = \frac{1}{3}$. For elongated spheroids $L_1 < \frac{1}{3}$, for flattened spheroids $L_1 > \frac{1}{3}$.

Repeating the calculation procedure carried out for a sphere, we get a system of equations for spheroids putting dipole moment of electrons $p_{i_\alpha} = e \cdot x_{i_\alpha}$ and using solution for stimulated oscillations $p_{i_\alpha} = p_{i_\alpha}(0) \cdot \exp(i\omega t)$:

$$\left(-\omega^2 + i\omega \nu_{0_i} + \omega_{0_i}^2 + \omega_{si_a}^2 \right) \cdot p_{i_\alpha} + \sum_{j \neq i} \omega_{sj_\alpha}^2 p_{j_\alpha} = \frac{e^2}{m} \cdot \frac{\varepsilon_0 E_\alpha}{\varepsilon_0 - L_\alpha (\varepsilon_0 - 1)}. \tag{33}$$

Solving the system on inhomogeneous algebraic equations allows us to calculate the effective permittivity of mixture containing ellipsoids with fixed axes ratio and same volume V:

$$\varepsilon_\alpha = \varepsilon_0(1-q) + q\left[1 + \frac{\varepsilon_0}{L_\alpha} \cdot \frac{\sum_i\left(\omega^2_{si_\alpha}\prod_{j\neq i} r'_j\right)}{\prod_i r'_i + \sum_i\left(\omega^2_{si_\alpha}\prod_{j\neq i} r'_j\right)}\right],\tag{34}$$

where $q = N_0 V$, $r'_i = \omega^2_{0_i} - \omega^2 + i\nu_{0_i}\omega$, N_0 is concentration of spheroids and

$$\omega^2_{si_\alpha} = \frac{\omega^2_{p_i} \cdot L_\alpha}{\varepsilon_0 - L_\alpha(\varepsilon_0 - 1)}.\tag{35}$$

To find natural frequencies of electron oscillations in spheroid, we use the equation (33) assuming its right part to be zero. The natural frequencies ω_α are found through solving a secular equation similar to (18):

$$\mathrm{Re}\left(Det\left|r'_i\delta_{ij} + \omega^2_{sj_\alpha}\right|\right) = 0.\tag{36}$$

Equation for ω_α determination of free electrons is reduced to

$$\left[\frac{\varepsilon_0 - L_\alpha(\varepsilon_0 - 1)}{L_\alpha} + \Delta\varepsilon_1(\omega_\alpha)\right] = \frac{\omega^2_p}{\omega^2_\alpha},\tag{37}$$

where $\Delta\varepsilon_1(\omega_\alpha)$ is contribution to the real part of dielectric permittivity ε' (14) determined by interband transitions, $\Delta\varepsilon_1(\omega_\alpha) = \mathrm{Re}\,\varepsilon' - 1$. Therefore,

$$\omega_\alpha = \omega_p\sqrt{\frac{L_\alpha}{\varepsilon_0 - L_\alpha(\varepsilon_0 - \varepsilon_M)}},\tag{38}$$

where $\varepsilon_M = 1 + \Delta\varepsilon_1(\omega_\alpha)$.

Let the natural frequencies be estimated for anelongated Ag spheroid with rotational axis $\alpha = x$. Assume that in (38) $\omega_p = 1.35 \cdot 10^{16}$ s^{-1}, $\varepsilon_0 = 2.25$, $\varepsilon_M = 4.5$ and axes ratio $b/a = 0.5$. It follows from (31) that $L_x = 0.17$ and $L_y = 0.5(1 - L_x) = 0.41$. Substituting specified values to (38) results in $\omega_x = 3.43 \cdot 10^{15}$ s^{-1} and $\omega_y = 4.85 \cdot 10^{15}$ s^{-1} while $L = 1/3$ and $\omega_F = 4.5 \cdot 10^{15}$ s^{-1}. The estimations reveal a considerable frequency splitting: ω_x is substantially shifted from ω_F in low-frequency direction while ω_y is slightly shifted from ω_F in high-frequency direction.

The natural frequency splitting results in a dependence of spectral position of absorption band maxima on the incident wave polarization E_α in colloidal solution of metal spheroids. Experimental studies confirm this conclusion. Thus, in [28], absorption spectra of colloidal gold solutions in high polymer matrix were studied. Basing on electronic photography, it has been established that oriented ellipsoidal golden particles are formed with the largest dimension $a << \lambda$. The absorption spectrum was studied in polarized light at polarizations $\mathbf{E}||X$ and $\mathbf{E}\perp X$ where X is the spheroid axis (Fig.2). It was established that at $\mathbf{E}||X$, a strong and wide absorption band arises with maximum in near infrared spectral region. At $\mathbf{E}\perp X$, there is a weak narrow band with maximum in visible region. The measurements revealed a substantial dichroism $\Delta D = D_{||} - D_\perp$ in near IR region and a possibility to use such composites in polarizer manufacturing. Authors also have calculated the absorption coefficients $K_{||}$ and $K_\perp$ at $b/a = 0.2$ using optical constants of gold and formulae for ε_{2ef} (similar to (8b)) generalized for the case of anisometric particles (Fig.3). The calculation reveals a considerable shift of $K_{||max}$ and negligible shift of $K_\perp$ as compared to K_{max} for a sphere. This agrees with estimated ω_x and ω_y values. It is also to note a significant difference between oscillator strengths f of $K_{||}(\omega)$ and $K_\perp(\omega)$ bands both in experiment and theoretical calculations. As it is shown in [16, 28], the difference is defined by a hybrid (combined) resonance predicting substantial weakening of oscillator strength $f \propto \int K(\omega)d\omega$ of high-frequency band when approaching the interband absorption edge.

Another example of anisometric Ag particle formation is known in photography. If a photoemulsion based on AgCl or AgBr is irradiated till appearance of coloration by colloidal Ag, and next irradiated by linearly polarized beam, then photoinduced dichroism appears. It was discovered by Weigert [29]. In subsequent researches, the dichroism was explained by formation of minute anisometric Ag particles oriented parallel or perpendicular to E_α. However, experimental verification of anisometric Ag particle existence in photoemulsions by means of electron microscopy is difficult because of the photoemulsion opacity for electron beam. Besides, Ag halides are decomposed under electron beam with large Ag particles being formed.

The causes of photoinduced dichroism have been clarified using thin-film samples prepared by thermal deposition in vacuum [30]. A thin granular Ag film was deposited on a heated glass substrate. Then the film was covered by AgI film, and the sample was irradiated by linearly polarized beam (with polarization E_0) of He-Ne laser ($\lambda = 633$ nm, $P \approx 50$ mW). Spectral studies using a linearly polarized (polarization E) test beam at $E| \ | E_0$ and $E \perp E_0$ gave two absorption bands: long-wave one at $E| \ | E_0$ and short-wave one at $E \perp E_0$. The dichroism was substantially larger than in photoemulsions (Fig.4). Silver iodide was then removed in fixing solution, and after that the measurements were repeated. The two bands remained but shifted towards the short-wave spectral region and weakened considerably. Electron-microscopic studies using fixed samples gave the following results.
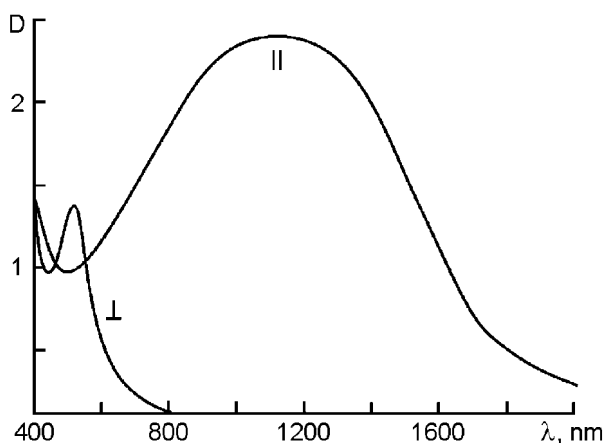

Fig.2. Absorption curves for a texture dichroic in infrared region of spectrum.
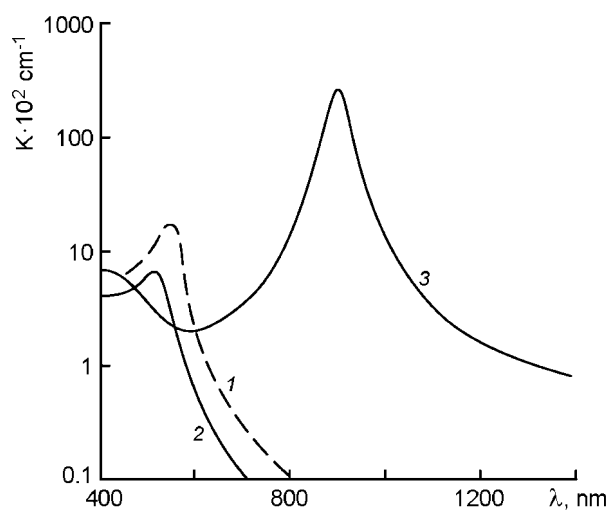

Fig.3. Absorption curves calculated for ellipsoidal golden particle at $b/a = 1$ (*1*), $K_\perp$ at $b/a = 0.2$ (*2*); $K_{| \ |}$ at $b/a = 0.2$ (*3*).

In initial unirradiated film, randomly situated minute (10 nm diameter) spherical Ag granules were observed, the filling factor being $q \approx 0.25$. After irradiation with polarized light, no elongated spheroids were observed. Instead, chains of spherical granules of 25 nm average diameter were observed. The chains were oriented mainly parallel to E_0, and filling factor for the irradiated film was $q \approx 0.17$ (see Fig.5). In thin granular films, the q factor was judged from area occupied by granules. The q factor decrease in two-dimensional colloid does not mean decrease of silver amount on the substrate. As electron microscopy measurements on 0.6 µm² area have shown, after irradiation the total volume of silver remains the same as before.

Absence of noticeable number of elongated particles in photographs and presence of oriented chains of spherical Ag granules points out the inapplicability of models proposed earlier [31] for explanation of Weigert effect in thin-film Ag-AgI system. We supposed that spherical granule in a chain is affected not only by external field but also by total field E_d created by adjacent granules in the chain. In dipole approximation, the total field can be represented as [32]
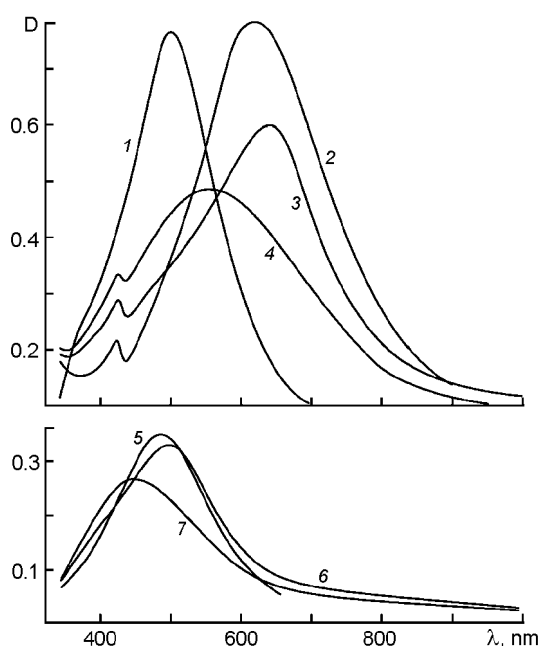
Fig.4. Absorption spectra of Ag-AgI and Ag films: *1*, initial film; *2*, Ag-AgI film treated by I_2 vapor; *3*, dichroic Ag film after irradiation by polarized laser beam ($\lambda = 633$nm), $\mathbf{E} \mid \mid \mathbf{E}_0$; *4*, $\mathbf{E} \perp \mathbf{E}_0$; *5*, Ag film after non-irradiated Ag-AgI treatment by fixing solution; *6*, dichroic Ag film obtained from irradiated and fixed Ag-AgI film, $\mathbf{E} \mid \mid \mathbf{E}_0$; and 7 for $\mathbf{E} \perp \mathbf{E}_0$.
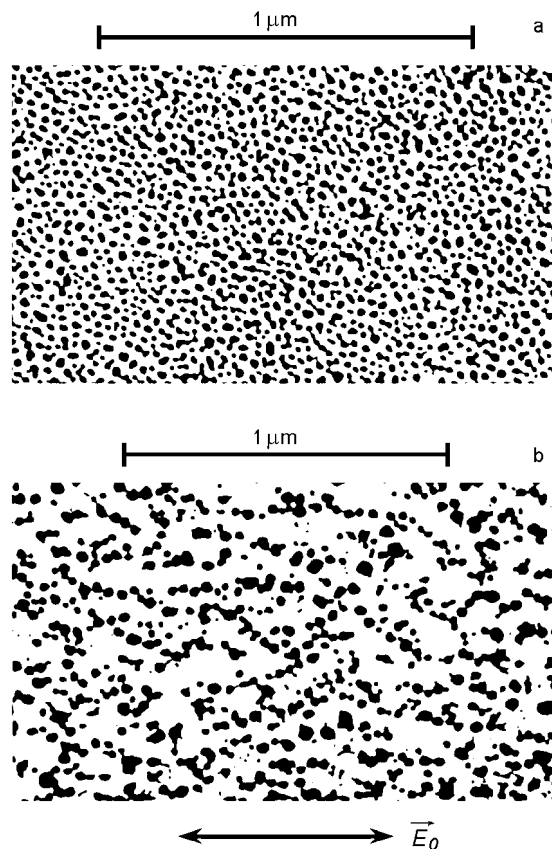
Fig.5. Electronic microphotographs of Ag films obtained after Ag-AgI film treatment by fixing solution: a) Ag film after fixing non-irradiated Ag-AgI film; b) dichroic Ag film after fixing Ag-AgI film irradiated by linearly polarized laser beam ($\lambda = 633$nm).

$$E_d = \frac{1}{\varepsilon_0} \sum_i \frac{1}{r_i} e^{ikr_i} \left\{ k^2 \left[\mathbf{p}_i - \mathbf{s}_i (\mathbf{s}_i \mathbf{p}_i) \right] + \frac{1 - ikr_i}{r_i^2} [3\mathbf{s}_i (\mathbf{s}_i \mathbf{p}_i) - \mathbf{p}_i] \right\}, \tag{39}$$

where summation is carried out for all granules in the chain, $\mathbf{p}_i$ is dipole moment of i-th granule, $\mathbf{s}_i = \dfrac{\mathbf{r}_i}{r_i}$, $k = \dfrac{2\pi}{\lambda} \sqrt{\varepsilon_0}$, r_i is distance between the i-th granule and specified one. The first item in braces is far-zone field, the second, the near-zone one. As the intergranular spacing in the chain is $b << \lambda$, the second "electrostatic" item contributes substantially to $\mathbf{E}_d$.

Let a test linearly polarized wave with field $\mathbf{E}_x \mid \mid \mathbf{E}_0$ and $\mathbf{E}_y \perp \mathbf{E}_0$ hits a chain (Fig.6). Here $\mathbf{E}_0$ is polarization vector of laser beam. Due to the measuring beam action, stimulated vibrations are excited in the chain. The vibrations are caused by total field $E_{x,y}(t) = (E_{x,y} + E_{d_{x,y}}) \exp(i\omega t)$ where $E_{x,y}$ is the incident wave field and

$$E_{d_x}(t) = \frac{2p_x}{\varepsilon_0 b^3} \sum_m \frac{1}{|m|^3}, \quad E_{d_y}(t) = \frac{p_x}{\varepsilon_0 b^3} \sum_m \frac{1}{|m|^3}, \quad m = \pm 1, \pm 2... \tag{40}$$

is the field from adjacent particles acting on the specified granule,

$$\mathbf{p} = \frac{4\pi Ne}{3} \cdot a^3 \mathbf{r}, \quad \mathbf{r} = x\mathbf{i} + y\mathbf{j} \tag{41}$$

is the metal sphere dipole moment. Considering polarization of the specified sphere under field

$E_{x,y}$, equations for vibrations of the specified sphere dipole moment take the form:

$$\ddot{p}_{x,y} + \nu \dot{p}_{x,y} + \omega_F^2 p_{x,y} = \frac{\omega_p^2 V}{4\pi} \cdot \frac{3\varepsilon_0}{\varepsilon_M + 2\varepsilon_0} \cdot (E_{x,y} + E_{d_{x,y}}) , \qquad (42)$$

where ω_F is the Frölich frequency; V , the sphere volume. Substituting (40) and (41) into (42) and passing to algebraic equations results in the following natural vibration frequencies of spheres in chain:

$$\omega_x \equiv \omega_{| |} = \omega_F \sqrt{1 - 2\left(\frac{a}{b}\right)^3 \sum_m \frac{1}{|m|^3}} , \quad \omega_y \equiv \omega_\perp = \omega_F \sqrt{1 + \left(\frac{a}{b}\right)^3 \sum_m \frac{1}{|m|^3}} . \qquad (43)$$

Using the definition $\mathbf{p} = \alpha \mathbf{E}$, we get also the complex polarizability of the sphere under electric field of specified frequency and polarization:

$$\alpha_{| |,\perp} = \frac{\omega_F^2 \varepsilon_0 a^3}{\omega_{| |,\perp}^2 - \omega^2 + i\nu\omega} . \qquad (44)$$

It follows from (43) that $\omega_{| |} < \omega_F$, $\omega_\perp > \omega_F$, and $\omega_{| |,\perp}$ substantially depends on the a/b ratio. As estimations reveal, the frequency splitting is noticeable within limits $0.1 < a/b < 0.5$. It is seen also that the largest contribution to the difference between $\omega_{| |}$ and $\omega_\perp$ is provided by particles adjacent to the specified one ($m = \pm 1$). Experimental data are in qualitative agreement with these results. Indeed, the absorption band at $E_{| |} = E_x$ is situated at lower frequencies as compared to $E_\perp = E_y$. But, as follows from Fig.4, $\omega_{| |} \approx \omega_F$ while $\omega_\perp$ is shifted from ω_F substantially. This contradiction may be explained by difference in filling factors q between unirradiated and irradiated Ag-AgI films ($q = 0.25$ and 0.17 , respectively).

Using the found polarizabilities $\alpha_{| |,\perp}$ for a sphere in chain, it is possible to calculate the polarization $P_{| |,\perp}$ of the medium containing chains, and to find $\varepsilon_{ef_{| |,\perp}}$ using (4). It is to note that at all the calculations, we have assumed constancy of a/b and a values and same chain orientation with respect to $\mathbf{E}$. In this case, the absorption band contour is close to Lorentz one. In real cases, however, there are fluctuations of these parameters resulting in $\omega_{| |,\perp}$ dispersion, i.e. to inhomogeneous broadening of absorption bands. At inhomogeneous broadening, the frequency distribution function $\psi(\omega_{| |,\perp})$ against parameter a/b should be known. This means that for more careful study of absorption spectra, microphotographs of samples are required. From the microphotographs, one can estimate $\psi(\omega_{| |,\perp})$ and describe contours of modified bands more precisely taking into account the distribution functions.

Influence of Nanoparticle Size on Optical Properties of Nanostructures. Mie effect

So far, we examined optical properties of composites containing nanostructures meeting the smallness criterion $k \cdot a \ll 1$. In this case, the electrostatic approximation is correct for many calculations, i.e. wave phase is constant within the particle. If the optical properties of composites are studied in visible region, then electrostatic approximation validity criterion is estimated to be $a \leq 20\,\text{nm}$. If nanoparticles are larger than 20 nm, then, the size increasing, transient light is increasingly attenuated due to scattering in composite.

As mentioned, a common spectrophotometric method of sample transmission measurements is used to study the absorption spectra of composites. Using this method and Bouguer law, the absorption coefficient K is determined. The same method with some improvements is used to study the transmission spectra of samples in which the light attenuation is defined not only by
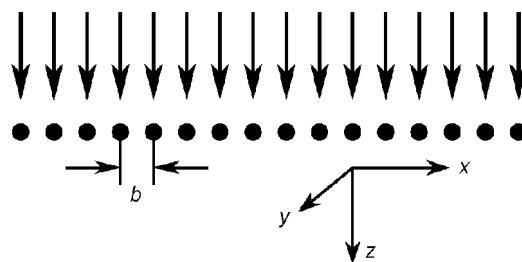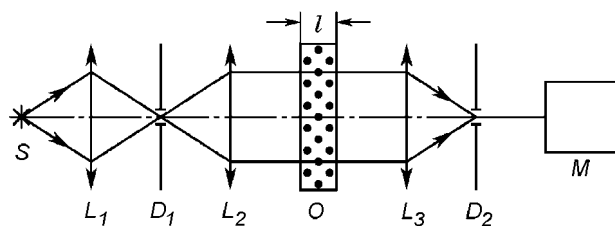
Fig.6. Model of chain of spherical Ag particles.

Fig.7. Optical scheme of extinction coefficient measurements. S is an extended light source; L_1, a lens focusing light on small aperture D_1; lens L_2 creates a parallel light beam, O, a plane-parallel sample to study; lens L_3 focuses light on small aperture D_2; M, a monochromator.

absorption but by scattering, too. A schematic diagram of such measurements is presented in Fig.7. An important component is the narrow aperture D_2. When a lens with focal distance F is used, a circular aperture of diameter d transmits the beams with angular aperture $\theta = 2F/d$. Usually $\theta_0 \leq 1°$ in such a scheme, and only a fraction of light scattered by the sample (scattered at $\theta \leq \theta_0$) hits the spectral instrument. If multiple scattering in the composite is neglected, the intensity of transmitted light can be described by means of Bouguer law

$$I = I_0 \exp\left(-K_{\text{ext}} \cdot l\right) \tag{45}$$

where K_{ext} is the extinction coefficient taking into account the light attenuation due to absorption and scattering of light forwards ($K_{\text{ext}} = K_{\text{abs}} + K_{\text{sca}}$). The extinction coefficient is connected with the light attenuation effective cross-section for a single particle:

$$K_{\text{ext}} = N_0 \cdot C_{\text{ext}}, \tag{46}$$

where the effective cross-section is $C_{\text{ext}} = C_{\text{abs}} + C_{\text{sca}}$, and N_0 is concentration of nanoparticles in the solvent.

Now let the principal concepts and formulae used in C_{ext} calculation be cited. To that end, we will follow the notation from [1, 7]. As scattered beams propagate in directions different from that of beam incidence, the concept of scattering plane is introduced. It is the plane constructed on wave vectors $\mathbf{k}_i$ and $\mathbf{k}_s$ of incident and scattered light, respectively. The incident wave electric field is resolved into two vector components: $\mathbf{E}_{i\parallel}$ parallel to scattering plane and $\mathbf{E}_{i\perp}$ perpendicular to the plane. Similar components of scattered wave are $\mathbf{E}_{s\parallel}$ and $\mathbf{E}_{s\perp}$. The connection between the field components of incident wave falling along Z axis and those of the scattered wave is defined by the amplitude scattering matrix [1]:

$$\begin{pmatrix} E_{s\parallel} \\ E_{s\perp} \end{pmatrix} = \frac{e^{i(\mathbf{kr}-kz)}}{-i\mathbf{kr}} \begin{pmatrix} S_2 & S_3 \\ S_4 & S_1 \end{pmatrix} \begin{pmatrix} E_{i\parallel} \\ E_{i\perp} \end{pmatrix}, \tag{47}$$

where $\mathbf{r}$ is radius-vector drawn to the observation point from the scattering particle of arbitrary size and shape situated at the coordinate origin, $\mathbf{k} \equiv \mathbf{k}_s$. The matrix elements S_i depend on meridional angle $\theta = \angle(\mathbf{k}_i, \mathbf{r}) = \angle(Z, \mathbf{r})$ and azimuthal angle φ counted from the scattering plane in the X,Y one. The formula (47) is suitable for particles of various shape, e.g. sphere, ellipsoid, cylinder, etc. From here on, we have restricted the problem to scattering on a metal sphere for which Mie theory has been developed.

When scattering occurs on a sphere, the amplitude matrix is simplified, since $S_3 = S_4 = 0$ and $S_1 = S_2 = S$. When determining the extinction coefficient (forwards scattering), $\theta \to 0$ and effective cross-section C_{ext} equals [1,7]

$$C_{\text{ext}} = \frac{4\pi}{k^2} \text{Re}\left[S(0°)\right]. \tag{48}$$

The Mie theory considers diffraction of plane wave hitting a metal sphere of arbitrary diameter and dielectric permittivity $\varepsilon' = \varepsilon_1 - i\varepsilon_2$ from a homogeneous transparent medium. Using boundary conditions for tangential components of $\mathbf{E}$ and $\mathbf{H}$, the field inside sphere and scattered field are found. The Mie theory details are given in [1, 7, 18]. Here we restrict ourselves to some conclusions from the Mie theory. At the sphere radius $a \to 0$, electrostatic approximation is suitable, the field inside the sphere is homogeneous, and the sphere behaves as an emitting dipole. As the radius

increases, the field inside sphere becomes inhomogeneous and concentrates at surface (surface modes), the scattering indicatrix becomes more complicated with maximum scattering along the incident wave direction. The Mie theory allows to calculate S_1 and S_2 matrix elements and their dependences on ε', a and meridional angle θ. In particular, at $\theta = 0°$,

$$S(0°) = \frac{1}{2}\sum_{n=1}^{\infty}(2n+1)(a_n + b_n),\tag{49}$$

where $n = 1,2,3...$ and form of a_n and b_n is found from Mie theory. Using coefficients a_n and b_n, the scattering cross-section is also found:

$$C_{sca} = \frac{2\pi}{k^2}\sum_{n=1}^{\infty}(2n+1)\left(\mid a_n \mid^2 + \mid b_n \mid^2\right),\tag{50}$$

coefficients a_n and b_n being expressed in terms of Riccati-Bessel functions:

$$a_n = \frac{m\psi_n(mx)\psi'_n(x) - \psi_n(x)\psi'_n(mx)}{m\psi_n(mx)\xi'_n(x) - \xi_n(x)\psi'_n(mx)},\ b_n = \frac{\psi_n(mx)\psi'_n(x) - \psi_n(x)\psi'_n(mx)}{\psi_n(mx)\xi'_n(x) - \xi_n(x)\psi'_n(mx)},\tag{51}$$

here $m = n'/n_0$, n' and n_0 are complex refractive index of the sphere and the surrounding medium refractive index, respectively; $x = \frac{2\pi}{\lambda}n_0 a$.

We are interested in K_{ext} for nanospheres, thus, the formulae (51) can be expanded in series with small parameters x and $\rho = mx$. The first members of expansion (up to x^6) look like

$$a_1 = -\frac{2ix^3}{3}\cdot\frac{m^2-1}{m^2+2} - \frac{2ix^5}{5}\cdot\frac{(m^2-2)(m^2-1)}{(m^2+2)^2} + \frac{4x^6}{9}\cdot\left(\frac{m^2-1}{m^2+2}\right)^2,\ b_1 = -\frac{ix^5}{45}(m^2-1)$$

$$a_2 = -\frac{ix^5}{15}\cdot\frac{m^2-1}{2m^2+3},\ b_2 = 0.\tag{52}$$

All the rest of a_n and b_n are zero at such an approximation. It is seen that expansion (52) may be used for most of metals at x up to $x^3 \approx 0.1$ ($x \approx 0.5$).

Substituting (51), (52) to formulae for C_{ext}, C_{sca} allows us to calculate the dependence $K_{ext}(\omega)$ and therefore to explain the experimental extinction spectrum against particle size. In the limiting case, $\mid\rho\mid <<1$, $b << a_1$, $S_1 = \frac{3}{2}a_1$, $S_2 = \frac{3}{2}a_1\cos\theta$, and, as follows from (50), (52) at $\theta = 0°$,

$$C_{sca} = \frac{8\pi}{3}k^4 a^6\left|\frac{\varepsilon'-\varepsilon_0}{\varepsilon'+2\varepsilon_0}\right|^2,\ C_{abs} = 4\pi k a^3\,\text{Im}\frac{\varepsilon'-\varepsilon_0}{\varepsilon'+2\varepsilon_0}.\tag{53a,b}$$

It is seen from (53) that the largest contribution to extinction is due to absorption by spheres. Formula (53b) is in accordance with formulae (7, 17) derived under electrostatic approximation. Fig.8 illustrates clearly the small contribution of C_{sca} to K_{ext} at $a = 20$nm. At the same time, the calculations using (51) reveal that at $a = 100$nm, the largest contribution to K_{ext} is due to light scattering. In [33], the Mie theory calculations are compared with experiment for the case of glasses containing Ag nanospheres. It has been shown that formulae (53) can be used up to $a = 45$nm, but it is necessary to consider particle size distribution which results in a substantial broadening of measured reflection spectra as compared to calculated ones.

Influence of Nanoparticles on Optical Properties of Surrounding Media and Particles

Metal nanoscaled particles differ considerably from bulk metals not only in optical properties. Electromagnetic fields generated in vicinity of nanoparticles may influence substantially the surrounding medium and particularly the adjacent molecules or solid surfaces.

It is small spheres that are of greatest interest in this regard because a dipole emission is typical thereof. If we interest in field acting on a molecule situated at distance $r > a$ from a dipole, then, as follows from (39), in addition to electrostatic field, a far-zone field is affecting the molecule:

$$\mathbf{E}_d = \frac{k^2}{\varepsilon_0 r}[\mathbf{s}[\mathbf{ps}]]\exp(-i\mathbf{kr}), \qquad (54)$$

where $\mathbf{p}$ is dipole moment induced in a sphere by external field, $\mathbf{p} = V\mathbf{P}$ (V is the sphere volume; $\mathbf{P}$, the medium polarization calculated by solving procedure of equations (15); r, the sphere to molecule distance; $\mathbf{s} = \mathbf{r}/r$). It follows from the double vector product in (54) that the electric field vector lies in a plane built on vectors $\mathbf{p}$ and $\mathbf{s}$, and at angle $\vartheta = \angle(\mathbf{p},\mathbf{s})$

$$E_d = \frac{k^2}{\varepsilon_0 r} \cdot p \cdot \sin\vartheta \cdot e^{-ikr}. \qquad (55)$$

The dipole moment induced in the sphere by an external field is

$$\mathbf{p} = \alpha\mathbf{E}_0 = a^3 \frac{m^2 - 1}{m^2 + 2}\mathbf{E}_0 = a^3 \frac{\varepsilon' - \varepsilon_0}{\varepsilon + 2\varepsilon_0}\mathbf{E}_0, \qquad (56)$$

where ε' is permittivity of the sphere metal. It follows from (54, 56) that at resonance conditions ($\text{Re}\varepsilon' = -2\varepsilon_0$), the field $\mathbf{E}_d$ near the sphere may reach large values both in far and near zones and may substantially exceed the incident wave field $\mathbf{E}_0$. If a molecule is situated close to the sphere or if the sphere contacts a solid surface, then $\mathbf{E}_d$ field may affect optical properties of the molecules or solids substantially. This may result in amplification of known effects or to appearance of new effects. Among various effects connected with field amplification by nanoparticles, the following are to be noted.

.1. Metal particles deposited on solid surface may considerably increase electron output from surface provided that photoelectric work function χ is below the plasma resonance frequency of the particle. Moreover, the photoelectric work function χ of nanoparticle put into a dielectric may be substantially lower than χ value for bulk metal. For instance, $\chi \approx 1.5\,\text{eV}$ for AgCl-Ag composite [34] while $\chi \approx 4\,\text{eV}$ at silver-vacuum boundary. As shown in [9], thin granular Ag films play a substantial part in electron emission from photocathode surfaces.
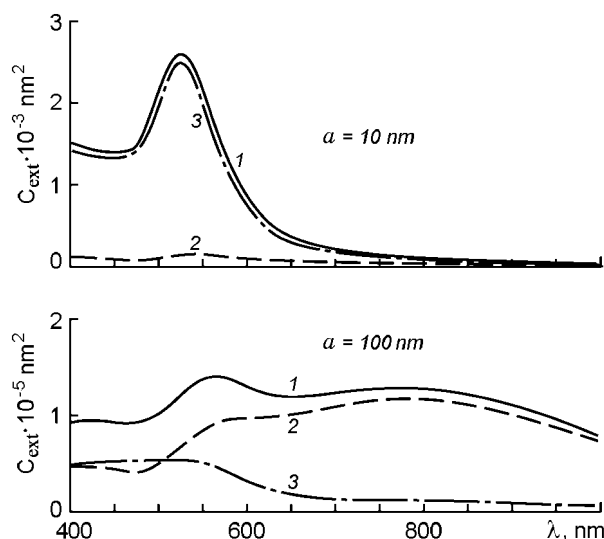
2. Ag nanoparticles favor the molecular monolayer luminescence amplification if the molecule absorption band is overlapped with resonant band of particles [35]. However, if a molecule contacts directly the metal particle or metal surface, then the luminescence is suppressed due to nonradiative transport of excited state energy from molecule to metal.

3. Amplification and generation of various nonlinear effects were discovered on metal surfaces and in granular metal films [36]. The

Fig.8. Calculated extinction (curve *1*), elastic scattering (*2*) and absorption (*3*) of isolated golden spheres of 20 and 100 nm radius.

second harmonic generation (SHG) is the best studied effect. It is to note that SHG should be observed only in center-nonsymmetrical bulk crystals [37]. But if the symmetry group of a substance includes inversion operation, then SHG may be observed on surface of such a substance due to its symmetry breaking near the surface. The same is true for granular metal films. Fig.9 illustrates SHG on silver films of various mass thickness d. The films were irradiated by YAG:Nd^{3+} laser beam ($\lambda = 1.06 \mu m$) and maximum of SHG generation is observed at $d \approx 4 nm$. Amplification of SHG is observed
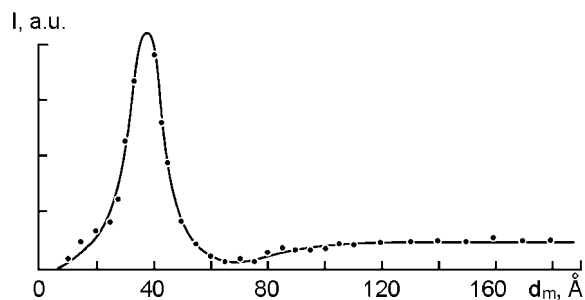

Fig.9. Second harmonic generation in granular silver films. Intensity of second harmonic generated by light at $1.06 \mu m$ wavelength as function of mass thickness.

because the SHG frequency is close to resonance frequency of Ag nanoparticle plasma vibrations. But as the film thickness increases, the film granularity disappears and SHG is attenuated.

4. Review of scientific literature shows that the largest number of works is aimed at the Raman scattering (RS) amplification by molecules situated near metal nanoparticles. It is experimentally found that RS is observed even on molecular monolayers covering the nanoparticles. This is a so-called giant Raman scattering (GRS) or amplified RS. Another name of this effect is surface-enhanced Raman scattering.

The GRS was studied under various conditions: for molecules in colloidal solutions of nanoparticles, on rough metal surfaces, on thin granular films deposited on various substrates. It was found that the largest GRS amplification is achieved on nanoparticles of small diameter ($a << \lambda$). Diameter a increasing, amplification drops due to local field reduction. The largest amplification coefficients achieved at GRS are of order of 10^6. The amplification coefficient depends on specific experimental conditions and on the nanoparticle metal. The most widely used metals are gold, silver, and copper due to their chemical inertness and favorable frequency dependence of optical constants in visible and near IR regions (small values $\varepsilon_2 = Im \varepsilon'$).

The full GRS theory is complicated enough. It needs studying interaction of fields induced by nanoparticle and molecule depending on molecule symmetry and disposition in near or far zone. The simplest theory is developed for a small sphere with dipole moment ruled by (56). As follows from (55, 56), the field of sphere is the largest at Frölich frequency ω_F and field intensity $I \propto \varepsilon_2(\omega_F)^{-1}$, see (12). In its turn, molecule under external field $\mathbf{E}_0$ behaves as a point dipole, its field acting on the sphere and may increase its polarizability. If RS is excited in the molecule with frequency $\omega_S = \omega_0 - \omega_k$ where ω_k is frequency of the molecular oscillatory mode, then $\mathbf{E}_S$ field being emitted by Stokes component affects the metal sphere, thus increasing its polarizability at ω_S frequency and intensity of GRS which is proportional to $|\alpha(\omega) \cdot \alpha(\omega - \omega_L)|^2$ [38]. In general, ω_k is lower than width $\Delta\omega \approx \gamma$ (26) of the sphere resonance band, i.e. both frequencies ω_0 and ω_S may be resonant.

It was also found that GRS is observed in spectrum of nanoparticle ensemble not complicated by presence of foreign molecules. The characteristic frequency shift of RS bands is $\Omega \approx 10 cm^{-1}$ in this case, $\Omega = \omega_S - \omega_0$. The bands were observed on rough metal surfaces with mean roughness of about 10 nm [39]. It was established that the bands are due to scattering on acoustic modes of metal (Brillouin scattering) amplified due to fields created by surface bulges.

The GRS phenomenon on molecules was discovered at late 70-ths of past century [40, 41]. Since then, the number of researches increased sharply. It is reasonable that the first researchers tried to fulfill the "purest" experimental conditions from the theoretical point of view. So in [42], colloidal solutions of silver and gold particles of 20 nm diameter developed before were used to observe GRS from pyridine molecules. The authors found an appreciable (by a factor of 5) amplification
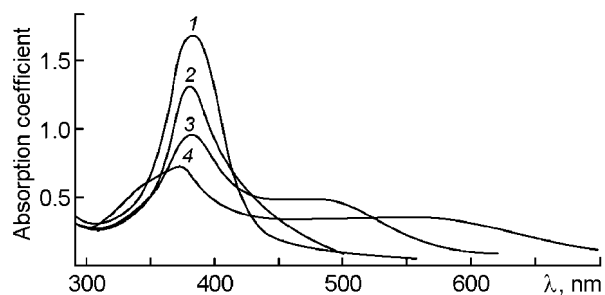
Fig.10. Extinction spectrum of silver-borane sol immediately after preparation (*1*), after increasing time intervals since pyridine addition (*2–4*).
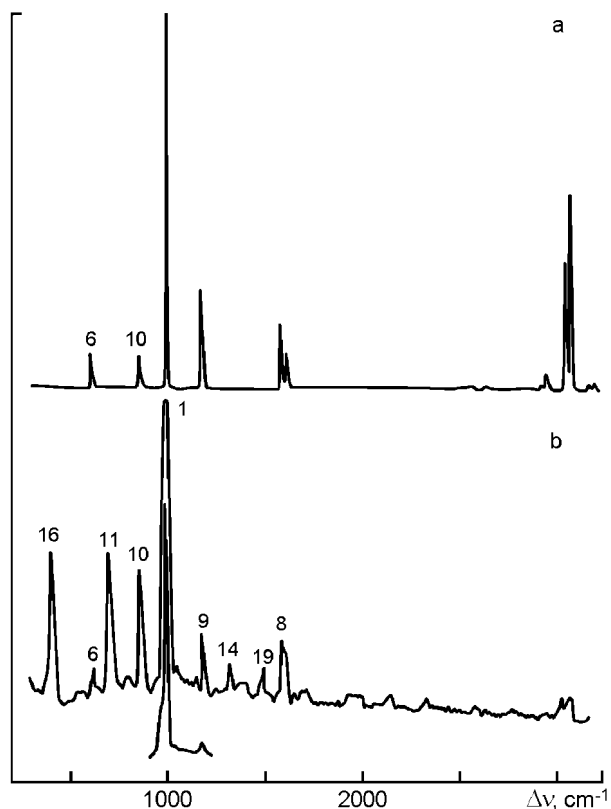

Fig.11. Raman scattering spectra of thick polycrystalline benzene film (a) and giant Raman scattering of benzene adsorbed on silver (b).

of pyridine RS as compared to water solution of the same molar concentration. However, persistence time increased, GRS amplification contour was found to be shifted in frequency. Tendency of Ag and Au particles to combine into chains and more complicated fractal structures was revealed basing on microphotos and extinction coefficient measurements (Fig.10). Just as at dichroism appearance in Ag-AgI composite (fig.4), two bands appeared in extinction spectrum. The frequency interval between the bands increased as the persistence time increased.

A low GRS amplification obtained in [42] is associated with small Ag and Au particle concentration in the colloidal solution. A substantially higher amplification (up to 10^6) is achieved in granular Ag films deposited on Al substrate and covered with molecular monolayers also deposited on substrates non-covered with granular Ag for comparison [43]. The authors studied GRS spectra of various simple molecules (ethylene, propylene, benzene) under irradiation by Ar^+-laser beam. The following facts were established. First, in addition to electromagnetic field from Ag particle, a chemical interaction of molecule and nanoparticle plays a part in GRS amplification. Second, at monolayer number increase, the GRS amplification coefficient decreases monotonously. Third, GRS spectrum may considerably differ from ordinary RS spectrum of the same substance. That is demonstrated by low-temperature GRS spectrum of benzene in comparison with polycrystalline benzene film spectrum (Fig.11). It is seen from the Figure that the GRS spectrum of molecules adsorbed on silver contains a number of lines absent in polycrystalline film, but some lines peculiar to benzene are weakened. The authors explain the appearance of new lines by symmetry of reduction benzene molecule deposited on silver. It is known that the point symmetry group of benzene molecule is D_{6h} which, in accordance with selection rules, defines appearance of RS lines corresponding to even vibrations relative to the inversion center. Owing to some reasons (Ag particle electromagnetic field action, chemical interaction with nanoparticles), the molecular symmetry is reduced to C_{3v} and selection rules peculiar to center-symmetrical molecule are violated.

A substantial GRS increase in granular Ag films stimulated studies on optical and structural properties of such films depending on the way of preparation, and works on their influence on GRS [44–46]. In those works, Ag films were prepared by vacuum deposition on unheated glass substrates and by subsequent annealing at various temperatures to obtain granular structure. The structure

was studied using AFM and X-ray structure analysis. It was found that film "ageing" influences the adsorbed molecules spectra and GRS amplification by adsorbed molecules [44]. A substantial dependence of GRS signal on the distance r between molecules and surface of Ag granule was found, too ($I \propto \left(\dfrac{a+r}{a} \right)^{-10}$, a being the granule radius) [45]. It has been established that the largest GRS amplification is achieved at the largest value of ratio of optical density in maximum of colloidal Ag absorption band to the band half-width [46]. The distance between Ag particles and particle heights are also of importance at GRS amplification.

The works cited point to the importance of GRS study. This phenomenon allows to research RS of substance in very small amounts, down to 10^{-8} mg. Such studies are often necessary at synthesis of new molecules, in studies of structure of biological molecules, etc. On the other hand, the first works [11] set a number of problems many of which are not solved yet: explanation of difference between GRS spectrum and usual RS spectrum in a bulk substance is often absent; the cause of GRS absence in the case of simple nonpolar molecules is not established yet, etc. Nevertheless, the number of works aimed at GRS increases steadily at a tendency to research the structure of multi-atomic molecules, polymer molecules of biological origin, etc.

The improvements in GRS observation procedures are also to be noted. Continuous gaseous and semiconductor lasers are suitable GRS excitation sources provided their frequency is in agreement with resonance frequency of nanoparticle plasma vibrations. Methods of regular nanostructure preparation by means of electron and laser lithography are being improved. One-dimensional and two-dimensional periodic structures with specified small periods and nanoparticle sizes are produced. Such structures are close in optical manifestations to photonic crystals [47, 48]. Technology of manufacturing the latter is improved and calculations of their energy spectra are improved more and more.

Conclusion

In this paper, the optical properties of nanostructures containing metal nanoparticles are briefly reviewed. Derivation of some simple formulae used when describing optical spectra of composites containing small particles of various form is presented. Theoretical statements are compared with experimental data. Some conclusions are discussed following from the Mie theory dedicated to diffraction on spheres of various diameter and dielectric permittivities. A number of examples of nanoparticle practical use and their action on surrounding medium is presented.

References

1. C.F.Bohren, D.R.Huffman, Absorption and Scattering of Light by Small Particles, Wiley, New York (1983).
2. U.Kreibig, M.Vollmer, Optical Properties of Metal Clusters, Springer-Verlag, Berlin, Heidelberg (1995).
3. L.D.Landau, E.M.Lifshits, Electrodynamics of Continuous Media. Gosizdatfizmatlit., Moscow (1959) [in Russian].
4. E.F.Venger, A.V.Goncharenko, M.L.Dmitruk, Optics of Small Particles and Disperse Media. Naukova Dumka, Kyiv (1999) [in Ukranian].
5. L.A.Golovan`, V.Yu.Timoshenko, P.K.Kashkarov, *Usp. Fiz. Nauk,* **177**, 619 (2007).
6. P.V.Meykliar, Physical Processes at Formation of Latent Photographic Images, Nauka, Moscow (1972) [in Russian].
7. G. Van de Huelst, Light Scattering by Small Particles, ILL, Moscow (1961).
8. G.V.Rosenberg, Optics of Thin-Layer Coatings, Gosizdatfizmatlit, Moscow (1958) [in Russian].
9. P.G.Borzyak, Yu.A.Kulyupin, Electron Processes in Island Metal Films, Naukova Dumka, Kiev (1980) [in Russian].
10. Surface Polaritons: A Collection of Works, ed. by V.M.Agranovich, D.L.Mills, Mauka, Moscow (1985), [in Russian].
11. Surface Enhanced Raman Scattering, ed. by R.Chang and T.Furtak, Plenum Press, New York and London (1982).
12. B.Karn, H.S.Matthews, *IEEE Spectrum,* **44**, 46 (2007).

13. V.Braun, Dielectrics, Berlin, Splinger-Verberg (1956).
14. P.Grosse, Free Electrons in Solids, Berlin, Splinger-Verlag (1979).
15. Color centers in Alkali Halide Crystals: A coll. of Works, ed. by A.S.Heinmann and K.B.Tolpygo, ILL, Moscow (1958).
16. V.K.Miloslavsky, I.N.Shklyarevsky, R.G.Yarovaya, *Opt. i Spektr.*, **46**, 303 (1979).
17. V.K.Miloslavsky, R.G.Yarovaya, *Opt. i Spektr.*, **21**, 309 (1966).
18. M.Born, E.Wolf, Principles of Optics, Pergamon press Oxford-London (1967).
19. J.C.Maxwell-Garnett, *Phil. Trans. Roy. Soc. (London)*, **A205**, 237 (1906).
20. D.A.G.Bruggermann, *Ann. Physik.*, 5 Folge, **24**, 636 (1935).
21. L.A.Ageev, V.K.Miloslavskii, E.D.Makovetskii, *Opt. i Spektr.,* **102**, 442 (2007).
22. L.A.Ageev, V.K.Miloslavsky, E.D.Makovetsky, et al., *Functional Materials,* **14**, 24 (2007).
23. K.S.Shifrin, *Izv. AN SSSR, Ser. Geofiz.*, No.2, 15 (1952).
24. M.Kerker, The Scattering of Light, Academic Press, New York, 1991.
25. L.A.Ageev, V.K.Miloslavsky, I.N.Shklyarevsky, in book: Dispersed Metal Films, ed. by Yu.A.Kulyupin, Inst. fiz. USSR, Kiev (1972) [in Russian].
26. W.A.Shercliff, Polarized Light, Harvard Univ. Press, (1962).
27. V.K.Miloslavsky, R.G.Yarovaya, L.A.Ageev, *Opt. i Spektr.*, **54**, 1044 (1983).
28. V.N.Lebedeva, G.I.Distler, *Opt. i Spektr.*, **23**, 963 (1967).
29. F.Weigert, *Zs. Phys.*, **2**, 1 (1920).
30. L.A.Ageev, V.K.Miloslavsky, I.N.Shklyarevsky, *Opt. i Spektr.*, **40**, 1024 (1976).
31. S.F.Cherdyntsev, *Zh. Fiz. Khim.*, **15**, 430 (1941).
32. L.D.Landau, E.M.Lifshits, Field Theory, Nauka, Moscow (1973) [in Russian].
33. W.T.Doyle, *Phys. Rev. B*, **39**, 9852 (1989).
34. K.Mies, T.James, Theory of Photographic Process, Chimiya, Leningrad (1973) [in Russian].
35. A.M.Glass, P.F.Liao, J.G.Bergman, D.H.Olson, *Opt. Lett.*, **5**, 368 (1980).
36. C.K.Chen, A.R.B. de Castro, Y.R.Shen, *Phys. Rev. Lett.*, **46**, 145 (1981).
37. Y.R.Shen, The Principles of Nonlinear Optics., Wiley, New York (1984).
38. D.S.Wang, H.Chew, M.Kerker, *Appl. Opt.*, **19**, 2256 (1980).
39. D.A.Weitz, T.J.Gramila, A.Z.Genack, J.I.Gersten, *Phys. Rev. Lett.*, **45**, 355 (1980).
40. M.Moskovits, *J. Chem. Phys.*, **69**, 4159 (1978).
41. M.G.Albrecht, J.A.Creighton, *J. Amer. Chem. Soc.*, **99**, 5215 (1977).
42. J.A.Creighton, C.G.Blatchford, M.G.Albrecht, *J. Chem. Soc. Faradey Trans II*, **75**, 790 (1979).
43. M.Moscovits, D.P.Dilella, *Chem. Phys. Lett.*, **73**, 500 (1980).
44. G.Vasilyuk, S.Maskevich, I.Sveklo et al., *J. Mol. Struct*, **410-411**, 223 (1997).
45. N.D.Strekal', A.E.German, G.A.Gachko, S.A.Maskevich, *Opt. i Spektr.*, **89**, 834 (2000).
46. G.T.Vasilyuk, *Vestnik GrGU (Belarus)* **2**, Ser. 2, 62 (2000).
47. I.D.Joannopoulos, R.D.Mead, J.N.Winn, Photonic Crystals. Molding the Flow of Light, Prinston Univ. Press (1995).
48. K.Sakoda, Optical Properties of Photonic Crystals, Springer-Verlag, Heidelberg (2001).

Оптичні властивості наноструктур

В.К.Милославський, Л.О.Агєєв, Є.Д.Маковецький, С.О.Маскевич

Представлено короткий огляд властивостей наноструктур, які містять металічні наночастинки. Наведено виводи деяких простих формул, що використовуються для опису оптичних спектрів композитів, які містять малі частинки різної форми. Проведено порівняння теорії з даними експерименту. Обговорюються наслідки, що витікають з теорії Мі, присвяченої дифракції на сферах різного діаметра та з різними діелектричними проникностями. Подано різноманітні приклади практичного застосування наночастинок та їхнього впливу на навколишне середовище.